Dimensional crossover in the superconducting intercalated layer compound $2H$-TaS_2

R. V. Coleman, G. K. Eiserman, S. J. Hillenius,* A. T. Mitchell, and J. L. Vicent†
Department of Physics, University of Virginia, Charlottesville, Virginia 22901
(Received 16 February 1982; revised manuscript received 19 August 1982)

The superconducting critical-field behavior of $2H$-TaS_2 single crystals intercalated with pyridine (PY), methylamine (MeA), dimethylamine (DMA), and ethylenediamine (EDA) has been measured in the field range 0—267 kG. The critical fields parallel to the layers for $2H$-TaS_2 intercalated with PY and MeA exhibit all of the features expected for crossover to two-dimensional behavior. A strong upward curvature in $H_{c2\|}$ vs T is present. A temperature-dependent critical-field anisotropy, $H_{c2\|}/H_{c2\perp}$, is observed which reaches values of ~ 60 for $T/T_c < 0.7$. The coupling constants are on the order of 1 and the data are all consistent with coherence lengths perpendicular to the layers that are less than the layer spacing. The data for $H_{c2\|}$ vs T have been analyzed using a computer fit to the theory of dimensional crossover developed by Klemm, Luther, and Beasley. The parameters generated by this fit are in complete agreement with values of these parameters calculated directly from the data and fully confirm the observation of complete dimensional crossover. Crystals intercalated with DMA and EDA show a less complete dimensional crossover and the computer-generated and calculated values of the parameters are not in agreement. This intermediate behavior is characterized by an anomalous upward curvature near T_c which cannot be systematically separated from the upward curvature due to dimensional crossover. The data presented on this entire group of intercalated layer compounds provide a complete analysis of the range of behavior observed and allow a critical evaluation of the case for observation of dimensional crossover. Discussion and analysis includes comparison to selected data on superconducting metallic intercalates as well as to other published data on organic intercalates.

I. INTRODUCTION

Layer-structure compounds[1,2] such as $NbSe_2$, TaS_2, and $TaSe_2$ are very anisotropic metals and exhibit a wide variety of electronic phase transitions, both in the pure crystal phase as well as in those produced by doping[3,4] or intercalation.[5,6] In the pure form, all of these compounds show transitions to a charge-density-wave (CDW) phase below some critical temperature. These transitions are associated with the favorable conditions for CDW formation[7] that result from the cylindrical shape of the Fermi surface and the accompanying Fermi-surface nesting. In addition, transitions to a superconducting phase are observed for most of the compounds and they provide good materials for studying the properties of anisotropic superconductors.

Pure $2H$-$NbSe_2$ is the best superconductor among the pure compounds, with a transition temperature of 7.2 K. The anisotropic behavior of the upper critical field has been studied extensively[8–10] and compared to models based on anisotropic Ginsburg-Landau (GL) theory. Pure $2H$-TaS_2 has a low superconducting transition temperature of 0.8 K and is somewhat more anisotropic than $2H$-$NbSe_2$, although both would be considered three-dimensional superconductors with relatively large anisotropies.

Intercalation of $2H$-TaS_2 with a variety of organic molecules has been found to produce a very substantial increase in the superconducting transition temperature[5,11] as well as a large increase in the observed anisotropy of the upper critical field. Transition temperatures in the range 3—6 K can be obtained and anisotropies are sufficiently large that a transition to a distinct two-dimensional behavior should be observable. The increase in layer separation and the decoupling of the layers suggested that Josephson tunneling perpendicular to the layers might play a role in the superconducting properties.

Katz[12] and Lawrence and Doniach[13] (LD) developed theories of the anisotropy based on the Josephson tunneling model and calculated properties within the context of anisotropic GL theory. More recently, Klemm *et al.*[14] have examined the problem in some detail and conclude that the Lawrence-Doniach equations predict the existence of a tem-

perature T^* below which the critical field parallel to the layers diverges to infinity. This temperature is defined as the temperature at which the coherence length $\xi_\perp(T^*)=S\sqrt{2}$, where S is the layer spacing. This apparent divergence predicted by the LD theory is a consequence of neglecting paramagnetic limiting and spin-orbit scattering in the layers. Klemm, Luther, and Beasley[14] (KLB) have extended the theory to include these effects and show that, although the divergence is removed, a dimensional crossover characterized by a strong upward curvature of $H_{c2\|}$ may still be observable. Previous experimental work by Prober *et al.*[15] on intercalated $2H$-TaS_2 showed upward curvature and a systematic trend toward dimensional crossover. In this paper we report on measurements of the critical-field anisotropy in $2H$-TaS_2 intercalated with a variety of organic molecules. Highly perfect crystals grown by special growth techniques have been used and the resulting intercalated crystals are systematically more perfect than those used in previous studies. The upper critical fields parallel to the layers exceed previously measured values, a strong upward curvature in $H_{c2\|}$ is observed, the critical-field anisotropy $H_{c2\|}/H_{c2\perp}$ is larger, and a temperature-dependent critical-field anisotropy is observed in all cases. Data have been taken in magnetic fields up to 267 kG and analyzed in terms of the KLB parameters.

The intercalates studied include pyridine (PY), C_5H_5N; methylamine (MeA), CH_3NH_2; dimethylamine (DMA), $(CH_3)_2NH$, and ethylenediamine (EDA), $H_2NCH_2CH_2NH_2$. The superconducting transitions in the intercalated crystals are reasonably sharp and examples are shown in Fig. 1. Table I lists the critical temperatures and layer spacings corresponding to the various intercalates. Data on $2H$-TaS_2 intercalated with Fe are also included for comparison.

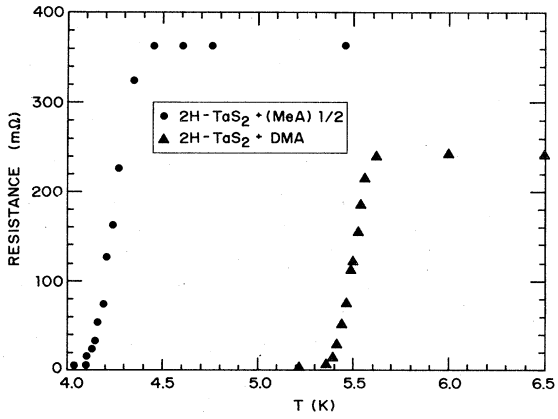

FIG. 1. Zero-field superconducting transitions observed in $2H$-TaS_2 intercalated with MeA and DMA. Transitions are ~0.2 K in width.

TABLE I. Material parameters measured for intercalated and unintercalated layered compounds.

Material	Layer separation[a] (Å)	T_c (K)	$1/\epsilon$
$2H$-TaS_2	6.04	0.8	6.0
$2H$-$NbSe_2$	6.27	7.1	3.3
$2H$-$TaS_2 + PY_{1/2}$	11.85	~3.6	≥50
$2H$-$TaS_2 + MeA_{1/2}$	9.24	~4.0	≥60
$2H$-TaS_2 + DMA	9.59	~4.6	≥28
$2H$-$TaS_2 + EDA_{1/4}$	9.53	~4.0	≥33
$2H$-$TaS_2 + Fe_{0.05}$	6.0	~3.0	≥20

[a]Layer spacings from Ref. 11.

II. EXPERIMENTAL PROCEDURE

Single crystals of $2H$- and $4Hb$-TaS_2 were prepared from stoichiometric prereacted powders using the iodine-vapor transport method. $4Hb$-TaS_2 single crystals were grown in a temperature gradient of 720—700 °C for four to six weeks and then quenched to room temperature. $2H$-TaS_2 crystals were formed by slowly cooling the $4Hb$-TaS_2 crystals from 700 °C to room temperature over a period of three days. This method of preparation of $2H$-TaS_2 produces crystals with residual resistance ratios as high as 200 and of sufficient quality to observe quantum oscillations in the magnetoresistance and susceptibility.[16] Intercalation of the crystals was carried out by sealing a crystal in a Pyrex tube with an excess of intercalate and then heating the tube in an oven for 5—48 h. Excess sulfur was also sealed into some of the tubes to prevent loss of stoichiometry. The temperatures necessary to achieve intercalation depend on the intercalate and are described in Ref. 11. Before and after intercalation the crystals were weighed and the thicknesses were measured. Weight gains and the increase in the dimension along the c axis were used to check for complete intercalation by comparing the changes to the data of Ref. 11. After intercalation, the crystals were cleaved and mounted on a printed circuit block using silver-paint contacts.

The temperature and field dependence of the resistivity were measured using standard four-lead dc techniques. Temperatures were maintained and measured below 4.2 K by immersing the sample in liquid helium and monitoring the vapor pressure. Above 4.2 K the temperature was maintained by mounting the sample on a heated copper block within a stainless-steel tube. The partial pressure of helium in the tube provided a thermal link with a liquid-helium or liquid-nitrogen bath. The temperature was measured using germanium and platinum

resistance thermometers.

Measurements in fields less than 70 kG were made in a superconducting solenoid. Measurements in fields up to 220 kG were made at the Francis Bitter National Magnet Laboratory at the Massachusetts Institute of Technology using Bitter solenoids. A few measurements on $2H$-$TaS_2 + MeA_{1/2}$ and on $2H$-$TaS_2 + PY_{1/2}$ have been extended to 267 kG using the new hybrid magnet at the Francis Bitter National Magnet Laboratory.

The upper critical fields $H_{c2||}$ were determined by extending the resistance transition curves to zero resistance, as indicated by the dashed lines in Fig. 7(b). This gives a lower limit on $H_{c2||}$. The midpoint of the resistive transition and the upper inflection point of the resistive transition have also been used for analysis, but no appreciable difference in the systematic trend is observed. All of the data presented here have been analyzed using the minimum $H_{c2||}$ which requires applied fields substantially greater than $H_{c2||}$ in order to complete the construction. Therefore, the values of $H_{c2||}$ plotted will be less than the experimental limit of the field sweep used to obtain them.

III. KLB THEORY

The anisotropic Ginsburg-Landau theory is generally valid only close to T_c where the coherence length perpendicular to the layers, $\xi_\perp(T)$, is much larger than the layer separation S. The more appropriate theory for the highly anisotropic layered superconductors is that of Klemm *et al.*[14] which is an extension of the Lawrence-Doniach model[13] based on Josephson tunneling between the layers.

Klemm *et al.*[14] have extended the LD model to include the effects of Pauli paramagnetism and spin-orbit scattering, and have developed expressions from which estimates can be made of the conditions necessary for observing crossover to a two-dimensional behavior characterized by a strong upward curvature in $H_{c2||}$. They do not limit the range of values for the parameters but assume that the dirty limit applies ($l \ll \xi_0$; $l =$ mean free path) for scattering processes within the layers and that the spin-orbit scattering rate is much less than the total scattering rate.

They have examined the detailed behavior of $H_{c2||}$ as a function of temperature for various values of the critical parameters involved. Orbital effects, Pauli paramagnetism, and the spin-orbit scattering time τ_{so} all affect the behavior of $H_{c2||}$. For certain ranges of the parameters, the combined effects can be expected to allow a dimensional crossover with an anomalous behavior of $H_{c2||}$. The interesting region will occur for strong spin-orbit scattering, $\tau_{so}T_c \ll 1$, and for weak interlayer coupling, coupling constant $r \approx 1$. Klemm *et al.*[14] have derived an expression for $H_{c2||}(T)$ near T_c and conclude that the upward curvature of $H_{c2||}$ will be most pronounced when the Pauli paramagnetic limiting effect is highly quenched by spin-orbit scattering. The most promising case for obtaining upward curvature corresponds to the extremely dirty limit with the electrons scattering many times in a given layer before tunneling to an adjacent layer.

The critical parameters of the theory, r, α, and $\tau_{so}T_c$, are related to the intrinsic superconducting parameters by the expressions given below. The parameter r, which characterizes the coupling strength between layers, is given by

$$r = \frac{4}{\pi}\left[\frac{\xi_\perp(0)}{S/2}\right]^2 , \tag{1}$$

where $\xi_\perp(0)$ is the zero-temperature coherence length perpendicular to the layers and S is the layer spacing. The value of $\xi_\perp(0)$ can be calculated from the expression

$$\xi_\perp(0) = \frac{\phi_0}{\xi_{||}(0)2\pi T_c \left|\frac{dH_{c2||}}{dT}\right|_{T_c}} , \tag{2}$$

where ϕ_0 is the flux quantum. $\xi_{||}(0)$ is obtained from a fit of the GL expression

$$\xi_{||}(T) = \xi_{||}(0)\left[\frac{T_c}{T_c - T}\right]^{1/2} \tag{3}$$

to the data. The values of $\xi_{||}(T)$ are calculated from the measured values of $H_{c2\perp}$ using the relation

$$\xi_{||}^2(T) = \frac{\phi_0}{2\pi H_{c2\perp}(T)} . \tag{4}$$

The parameter α describes the relative strength of the pair breaking due to Pauli paramagnetism (assuming no spin-orbit scattering) compared to that due to orbital effects, and is given by

$$\alpha \equiv \frac{\phi_0/2\pi\xi_{||}(0)\xi_\perp(0)}{4k_B T_c/\pi\mu_B} = \frac{dH_{c2||}/dT}{18.95\ \text{kG/K}} . \tag{5}$$

The parameter α can be estimated using the measured value of $dH_{c2||}/dT$ near T_c and will, of course, be consistent with a computer fit of the KLB theory to the same data.

The parameter $\tau_{so}T_c$ describes the spin-orbit scattering time, and is given by

$$\tau_{so}T_c = 2l_{so}/3\pi(1.17\xi_0) , \tag{6}$$

where l_{so} is the mean free path of the electron due to spin-orbit scattering. [$\tau_{so}T_c$ is a dimensionless

parameter and in this equation $\hbar = k_B = 1$ (Refs. 14 and 15).] No direct experimental determination of τ_{so} is available so $\tau_{so}T_c$ remains an adjustable parameter of the theory, although τ_{so} should be substantially greater than τ, the relaxation time estimated from the resistivity of the sample.

IV. EXPERIMENTAL RESULTS

The main result of KLB theory is an expression for $H_{c2||}$ vs T which can be fitted to the data using the parameters r, α, and $\tau_{so}T_c$. Such a fit has been made using an approximate set of equations and an adaptation of a computer program developed by Dalrymple.[17] For an equivalent set of parameters the resulting curves are very close to the theoretical plots given by Klemm *et al.*[14] for $H/(\pi\mu_B/4T_c)$ vs T/T_c. Data for all four organic intercalates diffused into $2H$-TaS_2 are presented below. The solid curves in all plots of $H_{c2||}$ vs T are calculated using the best set of parameters r, α, and $\tau_{so}T_c$ as determined by the computer fit to the data. Values of the parameters derived from the computer fit are listed in Table II. A brief summary of data obtained on the superconducting phase of pure $2H$-TaS_2 is also given.

A. Pure $2H$-TaS_2

Pure $2H$-TaS_2 is superconducting with a critical temperature of ~ 0.8 K. The angular dependence of the upper critical field at 0.4 K was previously measured[4] as shown in Fig. 2. With the use of anisotropic Ginsburg-Landau theory within the context of an effective-mass model, the angular dependence of the upper critical field can be expressed[8] as

$$H_{c2}(\theta) = \frac{H_{c2}(90°)}{(\sin^2\theta + \epsilon^2\cos^2\theta)^{1/2}}, \quad (7)$$

where $\epsilon^2 = m_{||}/m_{\perp}$ is the ratio of the effective mass parallel and perpendicular to the layers. The anisotropies observed for the various layered superconductors are conveniently compared using values of ϵ calculated from the best fit of the data to Eq. (7). The numbers listed in the tables and figures are values of $1/\epsilon$ which are also equal to the ratio of coherence lengths $\xi_{||}/\xi_{\perp}$ within the context of anisotropic Ginsburg-Landau theory. The value of this ratio for pure $2H$-TaS_2 is approximately 6.0, indicating a relatively mild anisotropy, but somewhat larger than the value of 3.3 observed[8] for pure $NbSe_2$. For both of these materials, ϵ was independent of temperature except very close to T_c.

TABLE II. KLB parameters determined from computer fits to $H_{c2||}$ vs T.

Material	α	r	$\tau_{so}T_c$
$2H$-$TaS_2 + PY_{1/2}$	2.48	0.77	0.026
$2H$-$TaS_2 + MeA_{1/2}$	2.96	0.85	0.02
$2H$-$TaS_2 + MeA_{1/2}$[a]	3.83	0.91	0.009
$2H$-TaS_2 + DMA	1.0	1.3	0.02
$2H$-$TaS_2 + EDA_{1/4}$	0.96	0.90	0.05
$2H$-$TaS_2 + Fe_{0.05}$	1.6	0.57	0.056
$2H$-$TaS_2 + PY_{1/2}$[b]	4.2	0.25	0.03

[a]Highest observed critical field (Fig. 7).
[b]Data taken from Ref. 19.

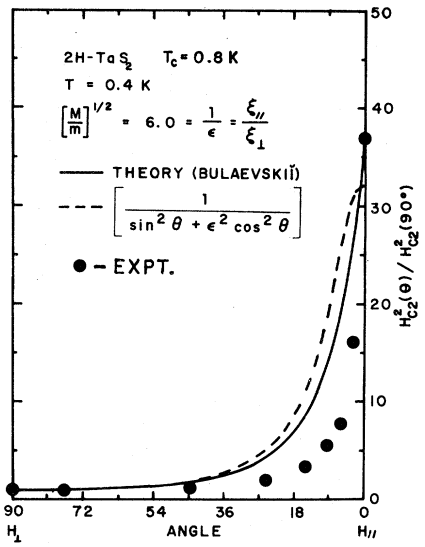

FIG. 2. Angular dependence of the upper critical field observed at 0.4 K for pure $2H$-TaS_2. The critical-field anisotropy and coherence-length anisotropy are on the order of 6. The angular dependence predicted by effective-mass theory and by a modified theory due to Bulaevskii (Ref. 22) are also shown. See Fig. 18 for the angular dependence observed after intercalation.

B. Intercalated $2H$-TaS_2

Intercalation of $2H$-TaS_2 with various organic molecules raises the superconducting transition temperature by as much as a factor of 5 and greatly enhances the critical-field anisotropy.[18,19] For the intercalated crystals with a sufficiently high superconducting anisotropy, the value of ϵ is temperature dependent and the effective-mass model breaks down. This is a reflection of dimensional crossover and leads to a temperature dependence of the perpendicular coherence length which reduces the coherence length to a value below the layer spacing and leads to a rapid upward curvature in $H_{c2||}$ versus temperature.

1. $2H$-$TaS_2+PY_{1/2}$

Pyridine-intercalated crystals have been studied extensively and much of the detailed data and analysis on the upper-critical-field anisotropy in intercalated layer compounds have been concerned with this material. Intercalation with pyridine raises the transition temperature into the range 3.7—4.0 K and increases the upper-critical-field anisotropy to values in the range 25—50. Previous experimental work[15,18] indicated a temperature-independent anisotropy and a relatively strong upward curvature in $H_{c2\|}$ vs T near T_c.

Our recent experiments with the more perfect crystals show an anisotropy of ~ 25 just below T_c, while at lower temperatures the anisotropy is temperature dependent and reaches a maximum value of ~ 50 at 2.5 K. The upper critical field parallel to the layers shows a very strong upward curvature below 3 K and reaches a value greater than 200 kG at 1.1 K, as shown in Fig. 3. The solid curve is a fit to KLB theory and gives parameters consistent with dimensional crossover, as listed in Table II and discussed in Sec. V.

The upper critical field perpendicular to the layers is shown in Fig. 4. An upward curvature is observed over the temperature range down to 1.1 K. This is present for all of the intercalates studied and seems to increase as the samples exhibit stronger characteristics associated with dimensional crossover. Below 1 K this upward curvature does not continue and a trend toward saturation of $H_{c2\perp}$ definitely occurs near 0.5 K, as shown in Fig. 4.

The upper-critical-field anisotropy $H_{c2\|}/H_{c2\perp}$ as a function of temperature is shown in Fig. 5. Just below T_c this starts at a value of ~ 20 and rises rapidly to a maximum of ~ 50 at 3 K. The rapid rise of $H_{c2\|}/H_{c2\perp}$ followed by saturation simply demonstrates the dominant influence of $H_{c2\|}$ vs T when strong upward curvature is present. The saturation is governed by the value of $\tau_{so}T_c$ which determines the curvature reversal of $H_{c2\|}$ vs T at low temperatures. $H_{c2\perp}$ shows anomalous upward curvature, but

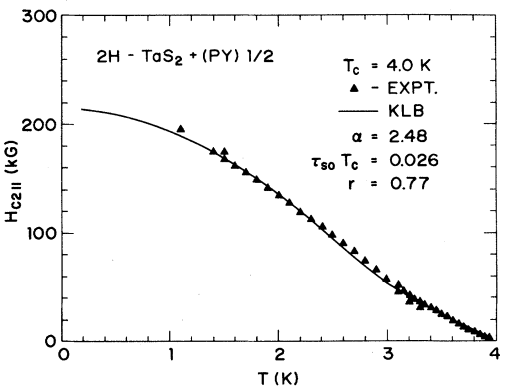

FIG. 3. Data recorded for $H_{c2\|}$ vs T for a single crystal of $2H$-TaS_2 intercalated with PY. The critical fields have been determined by measuring resistive transitions in fields up to 267 kG. The solid line is a computer fit of KLB theory to the data. See Fig. 7(b) for graphical determination of $H_{c2\|}$.

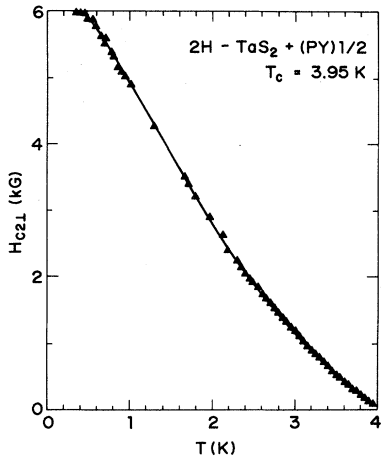

FIG. 4. Upper critical fields perpendicular to the layers measured for $2H$-$TaS_2+PY_{1/2}$ in the temperature range 4—0.4 K. Upward curvature is observed down to 0.8 K followed by saturation at lower temperatures.

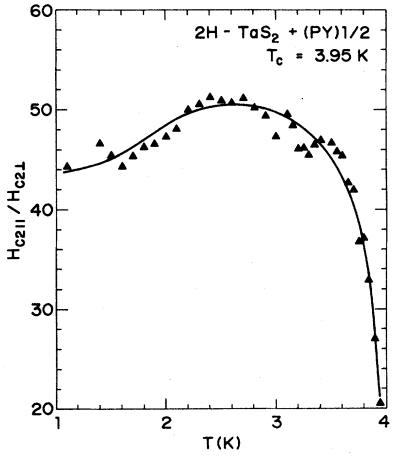

FIG. 5. Anisotropy of the upper critical field as a function of temperature observed for $2H$-$TaS_2+PY_{1/2}$. The rapid increase in anisotropy followed by saturation at lower temperatures is consistent with the behavior expected for dimensional crossover, as described by KLB theory. The anomalous upward curvature in $H_{c2\perp}$ vs T does not significantly influence the temperature dependence of $H_{c2\|}/H_{c2\perp}$.

the magnitude is too small to have any major effect on the overall temperature dependence of the anisotropy. The behavior of $H_{c2\perp}$ vs T suggests a subtle deviation from GL and further comments will be made on this feature in Sec. V.

2. $2H$-$TaS_2+MeA_{1/2}$

Methylamine-intercalated crystals show the largest critical fields so far measured for intercalated layer-structure crystals.[20] For a series of $2H$-$TaS_2+MeA_{1/2}$ crystals, the temperature dependence of $H_{c2\|}$ again shows a strong upward curvature with a value of T^* near 3 K. T^* is estimated to lie just below the onset of the strong upward curvature in the $H_{c2\|}$ vs T curve. T^* is defined as the temperature at which the divergence in $H_{c2\|}$ would occur if Pauli paramagnetism and spin-orbit scattering were neglected. Data for two different crystals taken in a field range of 0—267 kG and 0—150 kG, respectively, are shown in Fig. 6. The solid curves represent the best computer fit of the KLB theory to the data points.

The $2H$-TaS_2 crystals intercalated with MeA show instabilities to recycling from low temperature and the values of $H_{c2\|}$ can change from run to run. This introduces some difficulty in obtaining a complete set of data points for all field ranges using different magnets. However, strong upward curvature is systematically observed at ~ 3 K, and coupling constants in the range $r=0.85$—0.95 are consistently obtained. Data points for the specimen with the highest observed values of $H_{c2\|}$ are shown in Fig. 7(a) with zero resistance extending above 213 kG at 1.9 K, as shown in Fig. 7(b). The KLB fit, represented by the solid curve, gives a value of $r=0.91$. Values of $\tau_{so}T_c$ are less certain due to the small number of data points and the field limit of 213 kG, but this specimen clearly has a very large spin-orbit scattering. Three KLB curves are shown for three different values of $\tau_{so}T_c$ using the same value of $r=0.91$. Extension of the data using resistance transitions measured in fields to 267 kG at lower temperatures, as shown in Fig. 6(a), gives a more precise value of $\tau_{so}T_c$, but the corresponding values of $H_{c2\|}$ are lower than observed in the data of Fig. 7.

The perpendicular critical field $H_{c2\perp}$ vs T, as shown in Fig. 8, also shows an upward curvature of the same magnitude as observed for the pyridine intercalate. The critical-field anisotropy $H_{c2\|}/H_{c2\perp}$ grows rapidly below T_c and reaches a value of ~ 60 at 3 K, followed by saturation at lower temperatures as shown in Fig. 9. This again reflects the dominance of the $H_{c2\|}$ vs T behavior.

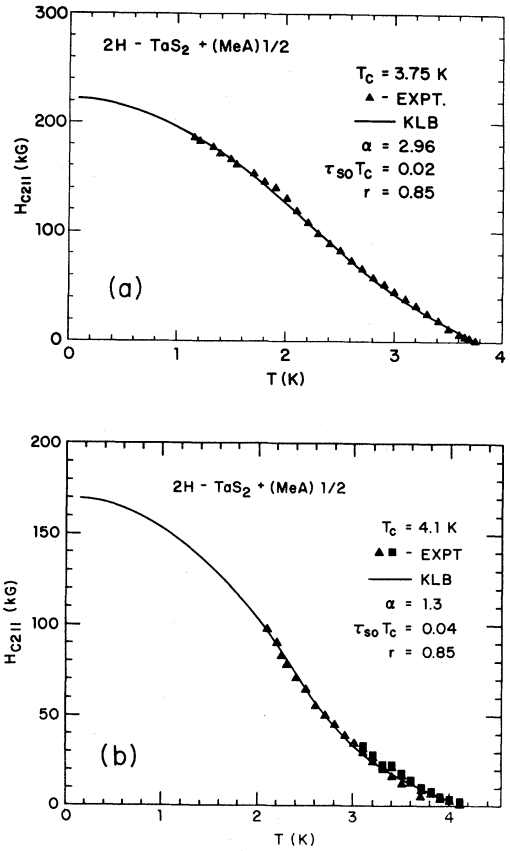

FIG. 6. Data recorded for $H_{c2\|}$ vs T for single crystals of $2H$-TaS_2 intercalated with MeA. (a) Field range 0—267 kG. (b) Field range 0—150 kG. Solid curves in both figures are generated by computer fits of KLB theory. Values of $H_{c2\|}$ are determined by the construction shown in Fig. 7(b).

3. $2H$-TaS_2+DMA

$2H$-TaS_2 intercalated with DMA, although exhibiting higher transition temperatures than $2H$-$TaS_2+MeA_{1/2}$, shows substantially lower critical fields and critical-field anisotropy. However, a strong upward curvature in $H_{c2\|}$ vs T and a temperature-dependent critical-field anisotropy are present. Figure 10(a) shows data on $H_{c2\|}$ vs T with T_c equal to 4.6 K and with the apparent T^* occurring below 3 K. The solid curve is again the best fit of KLB theory to the experimental points. The upper critical field $H_{c2\perp}$ also exhibits upward curvature as shown in Fig. 10(b). The anisotropy ratio $H_{c2\|}/H_{c2\perp}$ grows linearly with T_c-T, as shown in Fig. 11. No saturation is observed in this case, but

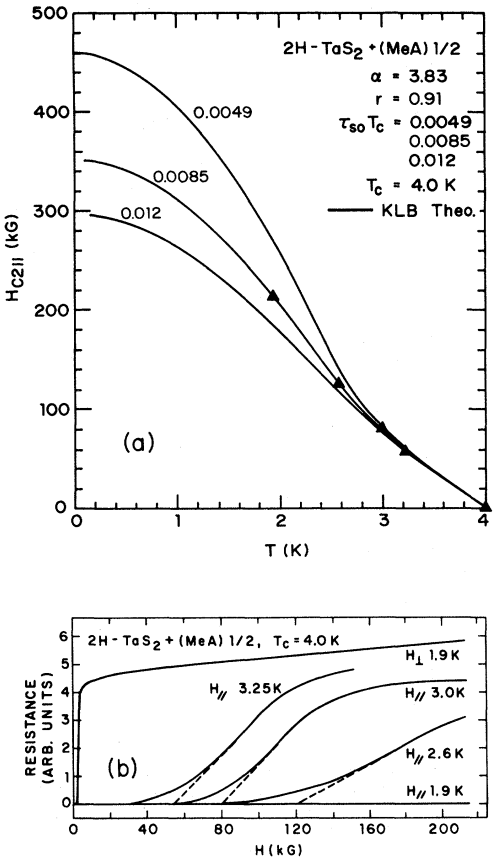

FIG. 7. Data recorded for a crystal of $2H$-$TaS_2 + MeA_{1/2}$ showing the highest critical field. (a) Data recorded for $H_{c2||}$ vs T. Experimental limit of 213 kG is exceeded at 1.9 K. Three KLB curves are shown with three different values of $\tau_{so}T_c$. The best fit is obtained with $\tau_{so}T_c = 0.0085$. (b) Field-induced resistive transitions observed for crystal analyzed in (a) above. The dashed line projection to zero resistance is used to determine $H_{c2||}$.

this is due to the lack of data at low temperature, $T \leq 1$ K, which would be needed to establish the inflection point in $H_{c2||}$ vs T.

The anisotropy for $2H$-TaS_2 + DMA is systematically lower than observed for the intercalates PY and MeA, even though the T_c is substantially higher. This is, however, consistent with the low apparent T^* observed for DMA. Since the layer spacing is comparable for MeA and DMA, 9.24 Å vs 9.59 Å, the source of this difference is either due to a high-temperature tail on $H_{c2||}$ vs T or to an intrinsic effect connected with differences in phonon structure or in electronic structure due to charge transfer to the layers from the intercalate. The initial slope $dH_{c2||}/dT$ near T_c is also substantially

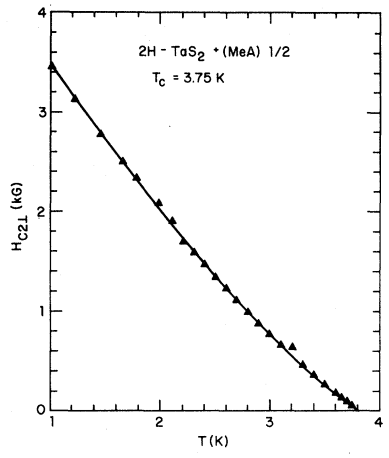

FIG. 8. Data recorded for $H_{c2\perp}$ vs T on $2H$-$TaS_2 + MeA_{1/2}$ crystal used for data recorded in Fig. 6(a). Upward curvature is observed over the entire temperature range 3.75–1 K.

lower than observed for the PY and MeA intercalates (see Table III).

4. $2H$-$TaS_2 + EDA_{1/4}$

The effects of EDA intercalation on the $2H$ phase of TaS_2 are similar to those observed for DMA. The upper critical field parallel to the layers versus temperature is shown in Fig. 12 for two different samples, one measured in fields up to 150 kG and one up to 70 kG. The solid curves represent the best fit of the data to KLB theory. The onset of upward curvature occurs just below 3 K, and the fit with

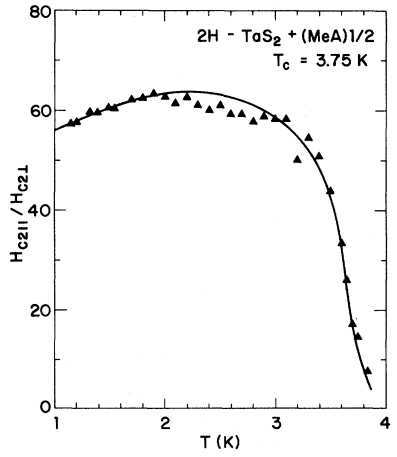

FIG. 9. Anisotropy of the upper critical field as a function of temperature observed for $2H$-$TaS_2 + MeA_{1/2}$. A rapid increase followed by saturation is observed as expected for dimensional crossover where $H_{c2||}$ vs T shows divergent behavior below T^*.

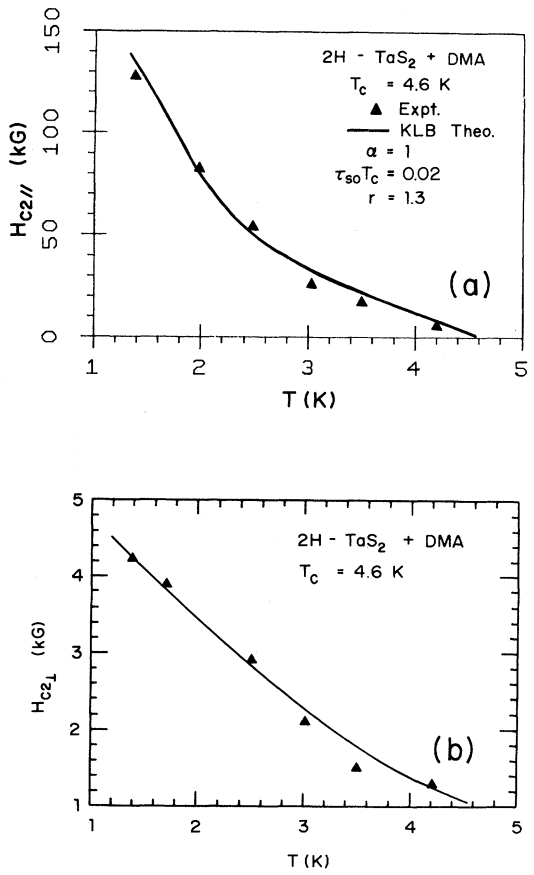

FIG. 10. Critical field vs T observed for $2H$-TaS_2 + DMA. (a) $H_{c2||}$ vs T in field range 0—150 kG. Solid curve is computer fit of KLB theory. (b) $H_{c2\perp}$ vs T. Upward curvature is again observed over the entire temperature range, but does not significantly alter the temperature dependence of $H_{c2||}/H_{c2\perp}$.

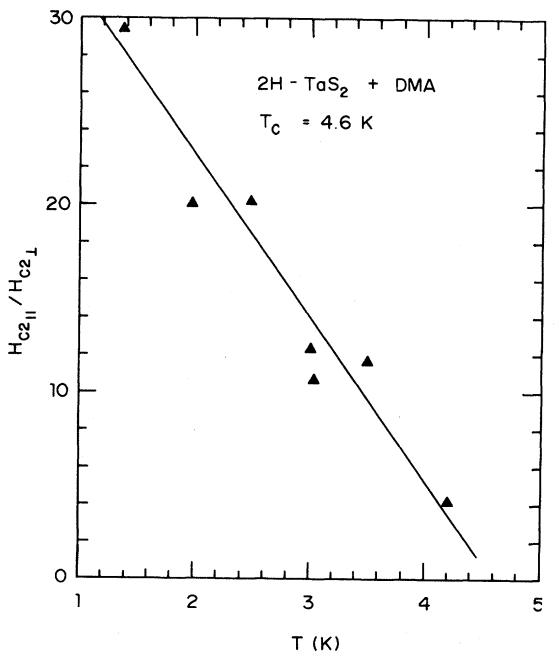

FIG. 11. Temperature-dependent anisotropy of the upper critical field observed for the specimen of $2H$-TaS_2 + DMA used to obtain the data in Fig. 10. This continues to increase as the temperature is lowered, but the data points provide less detail than in other runs and lower temperature points would be required for saturation.

KLB theory generates a coupling constant r slightly less than 1, compared to $r=1.3$ generated from the data on DMA intercalation. The upper critical field perpendicular to the layers also shows upward curvature, as shown in Fig. 13(a).

Although the decoupling and dimensional crossover appear to occur at lower temperatures than observed for PY and MeA intercalation, the crystal perfection and smooth resistive behavior suggest fairly perfect intercalation. The anisotropy is again temperature dependent, but shows a more abrupt break below the crossover temperature T^* than is observed for the other intercalates.

The onset of sharp upward curvature well below 3 K suggests a T^* much less than T_c as was the case for $2H$-TaS_2 + DMA. The critical-field anisotropy is again temperature dependent, with a sharp increase in anisotropy occurring below 3 K as shown in Fig. 13(b). The solid line in Fig. 13(b) has been calculated from the computer-generated KLB curve used to fit the $H_{c2||}$ vs T data of Fig. 12(a). This generates the saturation behavior although the data do not extend to low enough temperature to confirm

TABLE III. KLB parameters calculated directly from data.

Material	$\lvert dH_{c2\|\|}/dT \rvert_{T_c}$ (kG/K)	$\xi_\perp(0)$[a] (Å)	r[b]	α
$2H$-TaS_2 + $PY_{1/2}$	50.0	6.0	1.3	2.6
$2H$-TaS_2 + $MeA_{1/2}$	52.0	6.1	2.2	2.7
$2H$-TaS_2 + $MeA_{1/2}$[c]	77.5	4.0	0.91	4.1
$2H$-TaS_2 + DMA	19.5	24.0	32.4	1.0
$2H$-TaS_2 + $EDA_{1/4}$	15.4	21.0	24.8	0.5
$2H$-TaS_2 + $Fe_{0.05}$	34.5	13.7	25.6	1.6
$2H$-TaS_2 + $PY_{1/2}$[d]	78.0	5.0	0.8	4.2
$NbSe_2$[e]	23.3	26.0	87.0	1.2

[a]Calculated from Eq. (2).
[b]Calculated from Eq. (1).
[c]Highest observed critical field (Fig. 7).
[d]Numbers calculated using data in Ref. 19.
[e]Numbers taken from Ref. 15.

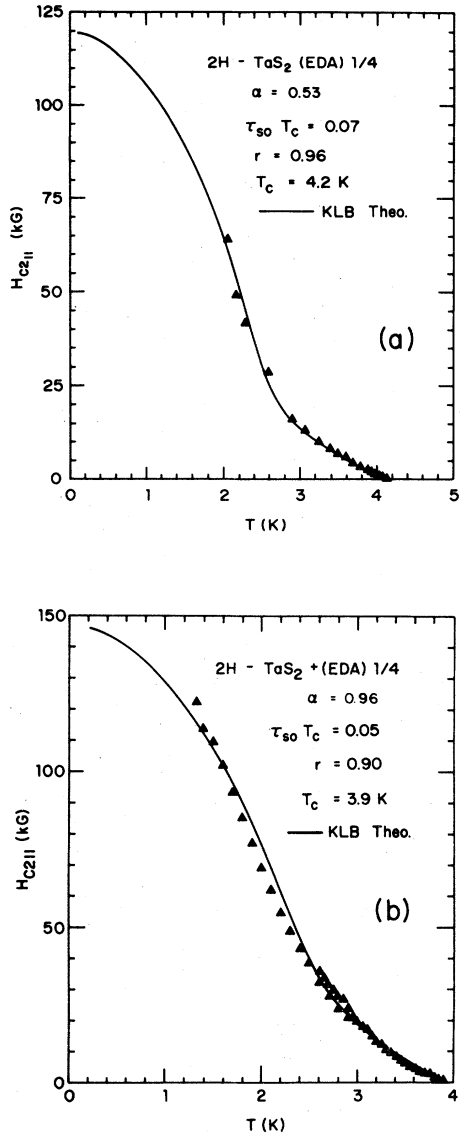

FIG. 12. Data recorded for $H_{c2\|}$ vs T for single crystals of $2H$-TaS_2 + $EDA_{1/4}$. Sharp upward curvature is observed below 3 K for both specimens. The solid curves are computer fits of KLB theory. (a) Field range 0—70 kG. (b) Field range 0—150 kG.

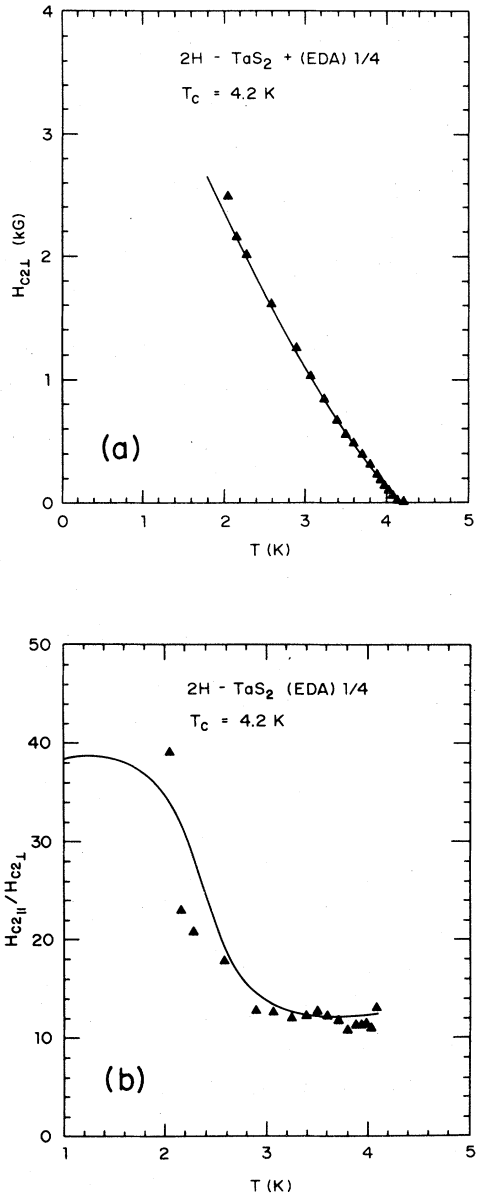

FIG. 13. (a) $H_{c2\perp}$ vs T recorded for $2H$-TaS_2 + $EDA_{1/4}$ crystal used for data in Fig. 12(a). Upward curvature is again evident over the measured temperature range. (b) Upper-critical-field anisotropy as a function of temperature observed for the same specimen. Solid curve has been generated from KLB theory and the data are consistent with a relatively low but sharply defined T^*. This uses the KLB parameters generated in Fig. 12 and shows the saturation although data do not extend to low enough temperature for confirmation.

it. This shows that the anisotropy data are consistent with KLB but do not, of course, add any new information other than that contained in the KLB fit to $H_{2c\|}$ vs T. The upward curvature is again present in $H_{c2\perp}$ vs T, as shown in Fig. 13(a), but is not of sufficient magnitude to have much effect on the temperature-dependent critical-field anisotropy. A similar behavior was observed for $2H$-TaS_2+analine by Prober *et al.*[15]

5. $2H$-TaS_2+Fe

The addition of Fe to $2H$-TaS_2 in the concentration range 0—6 at. % has been observed[21] to increase

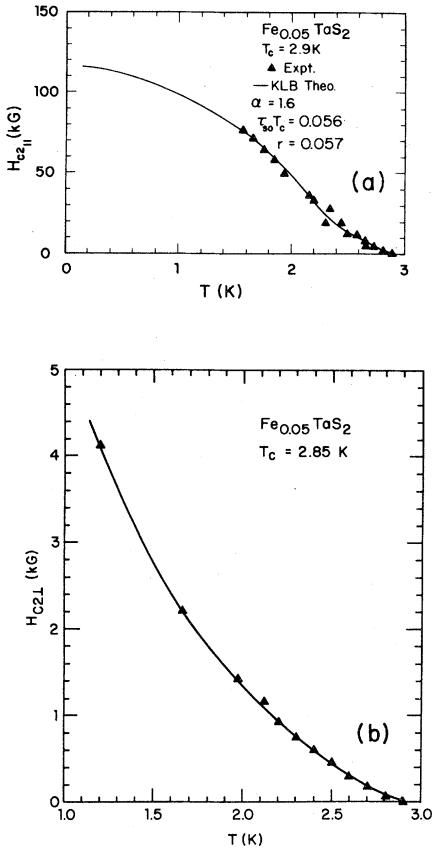

FIG. 14. Data on upper critical fields vs T recorded for single crystal of $2H$-$TaS_2 + Fe_{0.05}$. (a) $H_{c2||}$ vs T recorded in the field range 0—150 kG. Solid curve is a computer fit to KLB theory. (b) $H_{c2\perp}$ vs T. A strong upward curvature is also observed for this specimen and in this case produces a temperature-independent ratio $H_{c2||}/H_{c2\perp}$ as shown in Fig. 15.

the superconducting transition temperature to a maximum of ~ 3 K observed for $Fe_{0.05}TaS_2$. The critical-field anisotropy increases dramatically and upward curvature is observed in the plots of $H_{c2||}$ vs T, as shown in Fig. 14(a). This behavior is characteristic of that expected for a substantial decoupling of the layers, but the layer spacing is not changed significantly from that of the pure material and the role of dimensional crossover is less certain.

A computer fit of the KLB theory to the data for $H_{c2||}$ vs T is shown by the solid line in Fig. 14(a), and the computer-generated values of the parameters r, α, and $\tau_{so}T_c$ are clearly in the range expected for dimensional crossover. However, the value of r computed independently from Eq. (1) using the directly measured experimental properties is ≈ 25, much larger than the value $r=0.57$ derived from the computer fit. This will be discussed in more detail

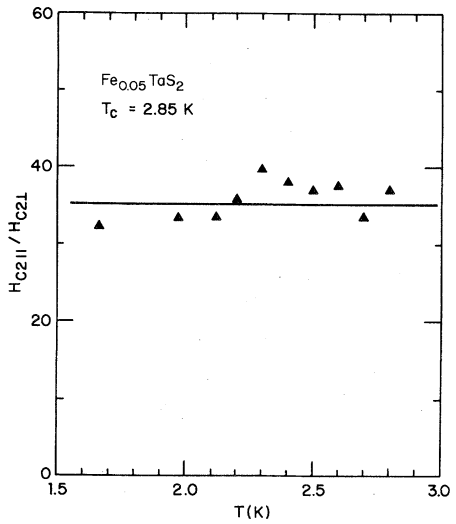

FIG. 15. Critical-field anisotropy as a function of temperature observed for $2H$-$TaS_2 + Fe_{0.05}$. The anisotropy is large, ≈ 38, but is independent of temperature. This is related to the unusually large curvature in $H_{c2\perp}$ vs T as shown in Fig. 14(b).

in Sec. V.

As shown in Fig. 14(b), the temperature dependence of $H_{c2\perp}$ for $Fe_{0.05}TaS_2$ also shows a distinct upward curvature. However, in contrast to the organic intercalates, this curvature is sufficiently strong so that the critical-field anisotropy is independent of temperature, as shown in Fig. 15.

V. DISCUSSION

The observation of upward curvature in $H_{c2||}$ vs T is a strong requirement of dimensional crossover, but does not alone confirm its presence. All of the intercalated specimens show strong upward curvature and the computer fits to KLB give values of the coupling constant r on the order of 1.

In order to establish a clear case of dimensional crossover, several other checks on the experimental behavior can be made. The observation of a strong temperature dependence in the critical-field anisotropy, $H_{c2||}/H_{c2\perp}$, can be used to show that $H_{c2||}$ is clearly diverging relative to $H_{c2\perp}$ below some temperature T^*. The coupling constant r can also be calculated directly from Eq. (1) provided a good estimate of $\xi_\perp(0)$ can be obtained. The coupling constant obtained from such a calculation should be in reasonable agreement with the coupling constant generated by the computer fit of the KLB theory to the data. (See Tables II and III.)

Equation (2) can be used to calculate $\xi_\perp(0)$ assum-

ing that a good value of $\xi_{||}(0)$ can be derived. This can be done using the GL expressions (3) and (4) if $H_{c2\perp}$ and $\xi_{||}(T)$ follow GL over the entire temperature range. The presence of the anomalous upward curvature in $H_{c2\perp}$ vs T indicates that this is not entirely true, but an estimate of $\xi_{||}(0)$ can still be made as shown in Fig. 16(a) for $2H$-$TaS_2 + PY_{1/2}$.

The data points are derived using Eq. (4) while the solid curve is the best fit of Eq. (3) to these points using $\xi_{||}(0)$ and T_c as adjustable parameters. The points clearly deviate from the exact GL temperature dependence of Eq. (3), but the deviation does not appear great enough to significantly alter the value of $\xi_{||}(0)$ for purposes of estimating $\xi_{\perp}(0)$ using Eq. (2).

In the case of $2H$-TaS_2 intercalated with PY and MeA the values of $\xi_{\perp}(0)$ derived using the above procedure are 6.0 and 6.1 Å, respectively, both substantially less than the layer spacing. When substituted in Eq. (1), the corresponding values of r are 1.3 and 2.2, somewhat larger than the values of r generated from the KLB fits but within the range consistent with dimensional crossover.

The major experimental characteristic assigned to dimensional crossover is the upward curvature observed in $H_{c2||}$ vs T. In $2H$-$TaS_2 + PY_{1/2}$ and $2H$-$TaS_2 + MeA_{1/2}$ this is a dominant characteristic, as shown by the strong temperature dependence of the ratio $H_{c2||}/H_{c2\perp}$. At temperatures below T^*, the relation between $\xi_{\perp}(T)$ and $H_{c2||}(T)$ should therefore be expected to deviate from anisotropic GL theory, although no detailed theoretical relationships have yet been worked out for the two-dimensional regime.

In the context of the anisotropic GL theory, the values of $\xi_{\perp}(T)$ would be related to $H_{c2||}(T)$ by the expression

$$\xi_{\perp}(T)=\frac{\phi_0}{2\pi\xi_{||}(T)H_{c2||}(T)}\ , \tag{8}$$

where $\xi_{||}(T)$ would be calculated from data on $H_{c2\perp}$ using Eq. (4). In order to check the degree of deviation, we have plotted the data for $\xi_{\perp}(T)$ using Eq. (8) as shown in Fig. 16(b) for $2H$-$TaS_2 + PY_{1/2}$. The solid points are computed from Eq. (8) while the solid line is generated using the GL temperature dependence given below:

$$\xi_{\perp}(T)=\xi_{\perp}(0)\left[\frac{T_c}{T_c-T}\right]^{1/2}. \tag{9}$$

The appropriate T_c has been used and the curve has been required to fit the high-temperature data points where the GL theory should be valid. At lower temperatures, the points calculated from $H_{c2||}(T)$ values using Eq. (8) clearly deviate from the temperature dependence of Eq. (9). The analysis suggests that

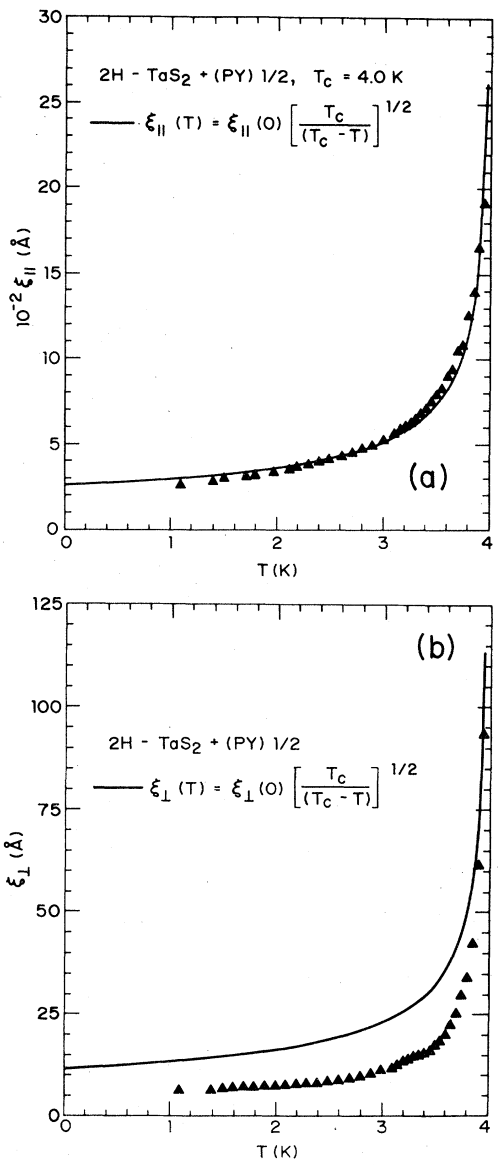

FIG. 16. Analysis of coherence length $\xi(T)$ vs T as derived from experimental measurements of critical fields for $2H$-$Tas_2 + PY_{1/2}$ and derived from the GL temperature dependences. (a) $\xi_{||}(T)$ vs T. Points are computed from the GL equation (4). The solid curve is a computer fit of Eq. (3) using $\xi_{||}(0)$ and T_c as adjustable parameters. Only a small deviation from GL is observed. (b) $\xi_{\perp}(T)$ vs T. Points are computed using GL equation (8). Solid line represents the GL temperature dependence of Eq. (9) calculated to fit the highest-temperature data point. $\xi_{\perp}(T)$ decreases more rapidly than predicted by GL theory.

the coherence length $\xi_{\perp}(T)$ falls more rapidly at low temperatures than predicted by the GL expression, although it should be remembered that Eq. (8) is not necessarily valid below T^*. The data on $2H$-

$TaS_2 + MeA_{1/2}$ behave in exactly the same way.

The same analysis has been made for $2H$-$TaS_2 + EDA_{1/4}$ and is shown in Fig. 17(b). In this case, the onset of upward curvature in $H_{c2\|}$ vs T was more abrupt and occurred at lower temperature; however, a strong deviation of $\xi_\perp(T)$ from GL theory is observed. In both cases the magnitude of $\xi_\perp(T)$ clearly approaches the layer spacing and deviates from GL theory in the direction expected.

Although the approximate analysis above indicates a deviation from GL theory in the temperature dependence of the perpendicular coherence length for all of the intercalates, the data for DMA and EDA when used in Eq. (2) do not generate values of $\xi_\perp(0)$ less than the layer spacing (see Table III). This is in contrast to the data on PY and MeA intercalates and is primarily due to the much lower values of $|dH_{c2\|}/dT|_{T_c}$ observed for DMA and EDA. The corresponding values of r calculated from Eq. (1) and listed in Table III are therefore much larger than those generated by the KLB fit to the $H_{c2\|}$ vs T data as given in Table II.

The reason for this discrepancy is not clear, but it may be connected with an anomalous tail on $H_{c2\|}$ vs T near T_c. In the case of $2H$-$TaS_2 + EDA_{1/4}$ this generates a region of temperature-independent anisotropy between 3 and 4 K [see Fig. 13(b)], which may not arise from a consistent extension of the superconducting behavior exhibiting dimensional crossover.

For the PY and MeA intercalates, a deviation from the effective-mass model is also observed in the angular dependence of the critical field. The effective-mass model predicts an angular dependence as given in Eq. (7) and represented by the solid curves in Fig. 18, where the ratio $H_{c2}^2(\theta)/H_{c2}^2(90°)$ has been plotted as a function of angle between the magnetic field and the plane of the layers. At low temperatures the observed critical fields as a function of angle clearly deviate from the effective-mass model for angles less than $\sim 8°$. This is further confirmation of the behavior which one might expect when the coherence length becomes on the order of the layer spacing and the fluxoid structure is modified. At temperatures close to T_c, this deviation is no longer present as shown for the lower curve in Fig. 18(b). The low-temperature deviations would also be well outside the limits of a modified angular-dependence model calculated by Bulaevskii[22] (see Fig. 3).

In the case of $2H$-TaS_2 + Fe, the critical-field anisotropy is independent of temperature over the entire measured temperature range. This is due in part to the strong upward curvature in $H_{c2\perp}$ vs T which effectively prevents any divergence between $H_{c2\|}$ and $H_{c2\perp}$.

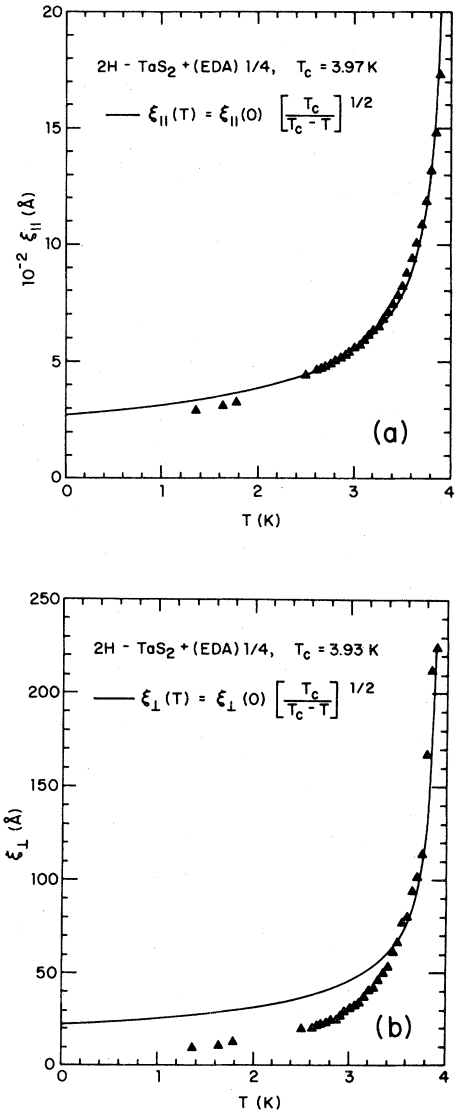

FIG. 17. Analysis of coherence length $\xi(T)$ vs T as derived from experimental measurements of critical fields for $2H$-$TaS_2 + EDA_{1/4}$ and derived from the GL temperature dependences. (a) $\xi_{\|}(T)$ vs T. Points are computed from the GL equation (4). The solid curve is a computer fit of Eq. (3) using $\xi_{\|}(0)$ and T_c as adjustable parameters. Only a small deviation from GL theory is observed. (b) $\xi_\perp(T)$ vs T. Points are computed using GL equation (8). Solid line represents the GL temperature dependence of Eq. (9) calculated to fit the highest temperature data point. $\xi_\perp(T)$ decreases more rapidly than predicted by GL theory.

The temperature dependence of $\xi_\perp(T)$ and $\xi_{\|}(T)$ for $2H$-TaS_2 + Fe has also been compared to GL theory, as shown in Fig. 19, and in this case deviations from the GL temperature dependence seem to be significantly less than observed for the organic

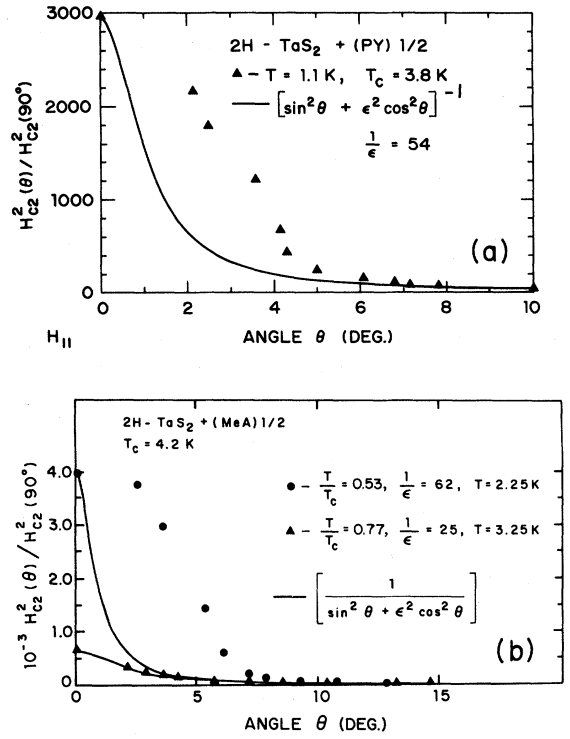

FIG. 18. Angular dependence of critical fields observed for angles close to orientation parallel to the layers. Below T^* in the more perfectly intercalated crystals we observe an abrupt departure from the effective-mass model at angles below 8°. (a) $2H$-$TaS_2 + PY_{1/2}$. (b) $2H$-$TaS_2 + MeA_{1/2}$. At higher temperature the effective-mass model is more closely followed [see lower curve in (b)].

intercalates. Although upward curvature in $H_{c2\|}$ vs T is present and a KLB fit to the data generates parameters appropriate for dimensional crossover, the other checks on the data do not seem to support a decoupling of the layers to the degree observed in PY and MeA intercalates. This is a case where a reasonably strong upward curvature in $H_{c2\|}$ vs T and a reasonably good computer fit to the KLB theory should not be taken as confirmation of dimensional crossover. The absence of a temperature-dependent critical-field anisotropy and the absence of any substantial deviation from the GL temperature dependence of coherence length suggest that the mechanism producing the upward curvature may not be identical in all types of intercalates.

Data on MoS_2 intercalated with alkali-metal and alkaline-earth—metal intercalates published by Woollam and Somoano[23] showed reasonably strong upward curvature and temperature-dependent anisotropies. However, the low values of $|dH_{c2\|}/dT|_{T_c}$, and the low values of critical field lead to very high values for the calculated coupling constant. Accurate fits of the KLB theory to data on these later materials would also require data at higher fields and lower temperatures than recorded in the published experiments.

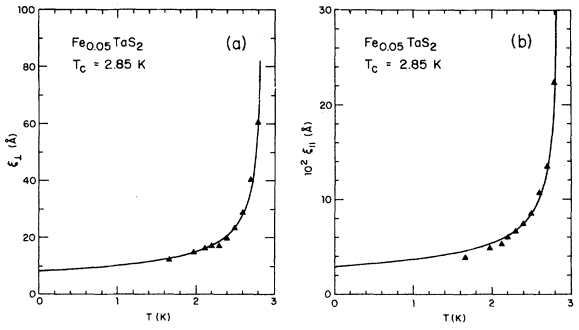

FIG. 19. Analysis of coherence length $\xi(T)$ vs T as derived from experimental measurements of critical fields for $2H$-$TaS_2 + Fe_{0.05}$ [see Eqs. (4) and (8)]. (a) $\xi_\perp(T)$ vs T. (b) $\xi_{\|}(T)$ vs T. In both cases the data fit the GL expressions quite well.

VI. CONCLUSIONS

For sufficiently perfect crystals of $2H$-TaS_2 intercalated with pyridine or with methylamine we have demonstrated that the superconducting critical-field properties are fully consistent with dimensional crossover as predicted by Klemm *et al.*[14] Upward curvature in $H_{c2\|}$ vs T, a temperature-dependent critical-field anisotropy $H_{c2\|}/H_{c2\perp}$, and a coherence length less than the layer spacing are all observed. The coupling constants derived from a fit to KLB theory and calculated directly from the relation

$$r=\frac{4}{\pi}\left[\frac{\xi_\perp(0)}{S/2}\right]^2$$

are both on the order of 1 which is well within the range required for dimensional crossover. For the specimens showing full dimensional crossover, the initial slopes at T_c, $|dH_{c2\|}/dT|_{T_c}$, are in the range 50—80 kG/K, giving values of α in the range 2.5—4.2. The upward curvature in $H_{c2\|}$ vs T also generates a temperature dependence of $\xi_\perp(T)$ which departs significantly from GL theory at low temperatures and shows the coherence length $\xi_\perp(T)$ dropping to much lower values than predicted by GL theory.

The observed critical-field behavior is extremely

sensitive to the preparation procedure and, although highly perfect selected crystals have been used in every intercalation, considerable variation occurs. For example, the three specimens intercalated with MeA as shown in Figs. 6 and 7 demonstrate the sensitive variation observed in KLB parameters and in T_c, even though all three crystals clearly exhibit behavior characteristic of dimensional crossover. Intercalated crystals showing less optimal critical-field properties develop a lower slope near T_c and substantially lower critical fields $H_{c2||}$ at low temperatures, although a strong upward curvature in $H_{c2||}$ vs T is still present. This anomalous curvature developing near T_c in the less optimal crystals merges with the curvature due to dimensional crossover and accurate separation is difficult.

The intercalates PY and MeA both give comparable results fully consistent with dimensional crossover, while DMA and EDA consistently show lower slopes near T_c and exhibit dimensional crossover characteristics at lower reduced temperatures. Similar crystals and procedures have been used for all of the intercalations and the resulting layer separation is approximately 9 Å except for pyridine which produces a 12-Å separation. This suggests that the detailed molecular structure in the layer is highly important although more information is needed on this factor.

The KLB theory is used as a three-parameter fit to the data and a high density of data points over the widest possible field range is required for generating a unique set of parameters. Data at 200 kG and above are necessary, particularly for generating a well-defined value of the spin-orbit scattering parameter $\tau_{so}T_c$. Data taken up to 267 kG on 2H-TaS_2 intercalated with PY and MeA give a highly convergent set of all three KLB parameters as indicated in Figs. 3 and 6(a). Crystals intercalated with MeA and PY with a higher intrinsic critical-field behavior, but measured to lower maximum fields as shown in Fig. 7(a), give convergent fits to KLB, but $\tau_{so}T_c$ is considerably less accurate. The value of this parameter is critical in determining the degree of divergence observed for $H_{c2||}$ and in the latter case one feels that the critical-field divergence might have been substantially greater and would have provided an even more limiting test for dimensional crossover and the KLB theory if higher-field points have been obtained. Unfortunately, the convergence of perfectly intercalated crystals and high-field magnets is hard to set up in advance. The high sensitivity of the optimal crystals to recycling and time deterioration make such experiments subject to a sensitive sequence of preparation and timing.

The present experiments demonstrate a major improvement in crystal quality and a clear transition into the critical-field regime expected for dimensional crossover. The results suggest that the ultimate limit in divergent critical-field behavior has not yet been reached and that further work could extend it. The overall framework of the dimensional crossover theory appears satisfactory, but a number of details need further investigation. For example, the upward curvature in $H_{c2\perp}$ vs T, the sudden departure of H_{c2} vs θ from effective-mass theory, and the departure of $\xi(T)$ vs T from GL theory represent experimental details which need further analysis. More work on the precise magnitude and analysis of the spin-orbit scattering parameter $\tau_{so}T_c$ should also be carried out.

---

*Present address: Bell Laboratories, Allentown, PA 18103.

†Present address: Universidad Complutense, Madrid 3, Spain.

[1]J. A. Wilson and A. D. Yoffe, Adv. Phys. 18, 193 (1969).

[2]F. J. DiSalvo, D. E. Moncton, J. A. Wilson, and S. Mahajan, Phys. Rev. B 14, 1543 (1976).

[3]S. J. Hillenius and R. V. Coleman, Phys. Rev. B 20, 4569 (1979).

[4]D. A. Whitney, R. M. Fleming, and R. V. Coleman, Phys. Rev. B 15, 3405 (1977).

[5]F. R. Gamble, F. J. DiSalvo, R. A. Klemm, and T. H. Geballe, Science 168, 568 (1970); F. R. Gamble, J. H. Osiecki, M. Cais, R. Pisharody, F. J. DiSalvo, and T. H. Geballe, *ibid.* 174, 493 (1971).

[6]D. E. Prober, M. R. Beasley, and R. E. Schwall, Phys. Rev. B 15, 5245 (1977).

[7]J. A. Wilson, F. J. DiSalvo, and S. Mahajan, Adv. Phys. 24, 117 (1975).

[8]R. C. Morris, R. V. Coleman, and Rajendra Bhandari, Phys. Rev. B 5, 895 (1972).

[9]S. Foner and E. J. McNiff, Jr., Phys. Lett. 45A, 492 (1973); P. de Trey, Suso Gygax, and J. P. Jan, J. Low Temp. Phys. 11, 421 (1973).

[10]N. Toyota, H. Nakatsuji, K. Noto, A. Hoshi, N. Kobayashi, Y. Muto, and Y. Onodera, J. Low Temp. Phys. 25, 483 (1976); P. de Trey, Suso Gygax, and J. P. Jan, *ibid.* 11, 421 (1973).

[11]S. F. Meyer, R. E. Howard, G. R. Stewart, J. V. Acrivos, and T. H. Geballe, J. Chem. Phys. 62, 4411 (1975).

[12]E. I. Katz, Zh. Eksp. Teor. Fiz. 56, 1675 (1969) [Sov. Phys.—JETP 31, 787 (1970)].

[13]W. Lawrence and S. Doniach, in *Proceedings of the Twelfth International Conference on Low Temperature Physics, Kyoto, 1970,* edited by Eizo Kanda (Academic, Kyoto, 1971), p. 361.

[14]R. A. Klemm, A. Luther, and M. R. Beasley, Phys. Rev. B 12, 877 (1975).
[15]D. E. Prober, R. E. Schwall, and M. R. Beasley, Phys. Rev. B 21, 2717 (1980).
[16]S. J. Hillenius and R. V. Coleman, Phys. Rev. B 18, 3790 (1978).
[17]Bruce J. Dalrymple (unpublished).
[18]R. C. Morris and R. V. Coleman, Phys. Rev. B 7, 991 (1973).
[19]M. Ikebe, K. Katagiri, Y. Watanabe, and Y. Muto, Physica (Utrecht) 105B, 453 (1981).
[20]J. L. Vicent, S. J. Hillenius, and R. V. Coleman, Phys. Rev. Lett. 44, 892 (1980).
[21]R. M. Fleming and R. V. Coleman, Phys. Rev. Lett. 34, 1502 (1975).
[22]L. N. Bulaevskii, Zh. Eksp. Teor. Fiz. 64, 2241 (1973) [Sov. Phys.—JETP 37, 1133 (1973)]; 65, 1278 (1973) [38, 634 (1974)].
[23]John A. Woollam and Robert B. Somoano, Phys. Rev. B 13, 3843 (1976).